This article has been published in Journal of Materials Engineering and Performance. The final publication is available at Springer via https://doi.org/10.1007/s11665-015-1480-7 .

Microstructure, macrosegregation and thermal analysis of direct chill cast AA5182 aluminum alloy

N. Jamaly, N. Haghdadi, A.B. Phillion
School of Engineering, The University of British Columbia, Kelowna, Canada

Abstract

The variation in microstructure, macrosegregation, and solidification behavior during aluminum alloy Direct Chill casting is investigated with respect to geometry. Optical microscopy, energy dispersive analysis and differential scanning calorimetry were employed to study the grain size evolution, distribution of alloying elements and solidification sequence across the cross-section of DC cast AA5182 aluminum alloy. The results show: (1) grain size increases from the surface to center of the ingot, corresponding to a decrease in the heat extraction rate; (2) there is a considerable macrosegregation of Mg, Mn and Cr, with Mg showing negative segregation at the center and positive segregation at the surface, Mn showing negative segregation both at center and surface and positive segregation elsewhere, and Cr showing positive segregation at the center and negative segregation at the surface; (3) thermal analysis of the as cast AA5182 also demonstrated that the solidus and the reaction temperatures vary as a function of position due to the local chemical composition and cooling rate. These findings, which show the interconnectivity of grain size, segregation and solidification sequence, are useful in further analysis of the DC casting process and in predicting casting-related defects, specifically hot tear formation.

Keywords: *Direct chill casting; Aluminum alloys; Grain size; Macrosegregation; Differential scanning calorimetry*

1. Introduction

Aluminum alloys are widely used in industry, particularly in the automotive and aerospace sectors, owing to their low density, high specific strength, appreciable corrosion resistance and great energy absorbency [1,2]. The main method for casting wrought aluminum alloys is the Direct Chill (DC) casting process, which produces cylindrical billets and rectangular ingots for subsequent processing in extrusion or rolling operations [3].

In recent decades, there has been great effort by researchers to better understand different aspects of the DC casting process as well as the microstructural properties of DC cast aluminum alloy products. Segregation of alloying elements, inhomogeneity of grain size, inclusions, porosity, and the formation of hot tears and cold cracks are some of the main issues usually associated with DC casting [4-7]. Hot tearing, in which a crack forms at temperatures

within the semisolid, has been particularly difficult to control [8]. In order to overcome these issues, various mathematical models have been developed. For example, Drezet et al. [9] examined dimensional instability of ingots using finite element (FE) analysis. Sengupta et al. [6] developed a comprehensive three-dimensional FE simulation to examine the effects of primary and secondary cooling during the start-up phase as well as cooling by the bottom block. Williams et al. [10] developed a multi-physics DC casting model coupling melt flow, stress and heat transfer. In each of these cases, the goal was to understand and predict the relationships between process parameters and the evolution in temperature and/or stress during casting. More recently, Jamaly et al. [11] studied the effect of microstructural features and process parameters on hot tearing formation during DC casting by coupling a novel semisolid constitutive law with a 2D thermal/stress DC casting model for AA5182.

The microstructural features of DC cast alloys have also been studied as a function of processing conditions. Macrosegregation along a cross-section of a DC cast billet was studied by Nadella et al. [12]. Eskin et al. [13] studied the effect of cooling rate and grain refinement on elemental distribution; low casting speeds were found to enhance positive segregation in DC cast billet independently of grain size while higher speeds required significant inoculation and thus grain refinement in order for positive segregation to occur. Effects of melt temperature and DC casting speed on hot tearing, dendrite arm spacing, grain size, eutectic volume fraction, porosity and segregation have also been studied, with a focus on Al-Cu alloys [14].

Wrought AA5182 aluminum alloy produced via DC casting is widely used in automotive components and for beverage cans. Although a number of mathematical models have been developed to understand and reduce distortions and hot tear formation, there have been only a few studies systematically examining alloy microstructure, and compositional variations. In one work, Glenn et al. [15] examined the effect of grain refiners on grain size, macrosegregation, and thermal conductivity. However, additional experimental study is needed to characterize the grain structure and solute re-distribution during DC casting. As shown by Jamaly et al. [11], knowledge of grain size and grain coalescence during solidification is key for predicting hot tearing. Furthermore, macrosegregation, if not controlled during casting, reduces the quality of the finished product.

Thermal analysis through differential scanning calorimetry (DSC) represents a powerful approach for studying multicomponent alloy solidification [16]. In the case of DC casting, DSC can be used to characterize the kinetics of solidification of specimens taken from different locations in the casting, which have different chemical compositions. Bearing this in mind, microscopy, composition mapping and thermal analysis have been combined in the

current study to provide new insight into the solidification kinetics, microstructure and macrosegregation of a DC cast AA5182 ingot.

2. Experimental methods

The experimental material was an AA5182 DC cast ingot section[1] from the steady-state regime, with a cross-section of 1650×510 mm, provided by Rio Tinto. A series of small cubic samples, 10 mm on a side, were cut from the centerline of the rolling face. In total, 5 samples were taken, from the center to the surface (0.0/center, 62.5, 125/middle, 187.5, and 250/surface mm). These samples were used for grain size measurements, chemical composition analysis and thermal (DSC) analysis.

Grain size: Measurements were carried out on each sample. Sample preparation took place by mounting with a thermosetting resin, grinding, then polishing down to a 1 µm finish with colloidal silica, then electrochemically etched using Barker's reagent to reveal the grain boundaries. The metallographs were then characterized using a Zeiss Axio optical microscope. Jeffrie's method was used to measure the size of grains based on the description given in ASTM E112 [17]. Briefly, a circle is drawn on a metallographic image with a magnification selected so that the circle partially/fully inscribes at least 50 grains. The grain density, N_A, is then obtained by $N_A = f(N_{inside} + \frac{N_{intercept}}{2})$, where N_{inside} is the number of grains completely inscribed by the circle, $N_{intercept}$ is the number of grains partially inscribed in the circle, and f is known as the Jeffries' multiplier, which is a function of magnification.

Chemical analysis: An Oxford Instruments X-max 80 mm^2 energy dispersive spectroscope (EDS) coupled to a Tescan Mira 3 field emission scanning electron microscope (SEM) and Oxford AZtec 2.0 analysis software was used to determine the composition of each sample. Specifically, an EDS signal was acquired on ~10 rectangular subregions, each with a dimension of 100×100µm. The compositions of each element from different locations within the same sample were then averaged to represent the bulk composition of that element within that sample. To ensure accuracy in the EDS results, we followed the requirements proposed by Newberry and Ritchie [18] for performing quantitative EDS.

Thermal analysis: Small specimens of ~20 mg were extracted from each sample for thermal analysis. DSC was performed using a Netzsch STA 449 F3 thermal analysis instrument

[1] The nominal composition, Al–3.92wt.% Mg–0.38wt.%Mn–0.18wt.%Cr, was determined by averaging the EDS measurements at individual locations presented in Table 2. The values of Mn and Cr fall within the alloy's specification. The value for Mg is below what is expected for AA 5182, 4-5 wt.%Mg.

in order to acquire the evolution in solid fraction with temperature. First, the instrument was calibrated using standards of In, Al, Ag, Au and Ni. Second, each specimen was placed into an alumina crucible within the DSC. The chamber was closed and then evacuated and purged with N_2 gas. Third, the testing cycle was programmed into the software, requiring the evolution in temperature with time to be specified. Specimens were first heated to 700˚C and then cooled to 400˚C at either 10 or 20 ˚C/min. To ensure that the results were reproducible, 3 specimens from each location were tested. The results were then analyzed using the Netzsch Proteus software.

3. Results and discussion

3.1 Grain size

Example microstructures selected from different locations from the center of the ingot out towards the surface along the centerline of the rolling face are shown in Fig. 1. As is seen, the grains are equiaxed dendritic in all locations, but with a grain size that changes significantly. Qualitatively, the highest grain size is obtained at the center and then the size of grains gradually decreases out to the surface. The quantitative measurements of grain size are given in Table 1. The measurements also confirm the qualitative observation; the average grain size in center is more than four times larger than the value found at the surface.

The observed grain size variation from center to surface is due to the variable cooling conditions experienced throughout the cross section of the ingot. At the surface, the rate of heat removal is high due to the primary mould interfacial cooling, resulting in small grains. This effect diminishes away from the surface, as the rate of heat removal is controlled by the rate of heat conduction through the casting, which diminishes the heat extraction rate. The observed decrease in grain size with increasing cooling rate can be then reasoned as follows. Increasing the cooling rate enhances both the nucleation potency of the inoculant in the melt and the density of active nucleation sites [19]. Since grain growth occurs at a uniform rate for a given set of cooling conditions, an increase in the nucleation density leads to the formation of finer grains.

In addition to the cooling rate effects, the local variations in chemical composition may also affect the grain size. It is generally accepted that increasing the solute concentration has a grain refinement effect by hindering grain growth through solute pile-up at the solid–liquid interface, enhancing grain nucleation due to the constitutional undercooling [20]. As is elaborated in the next section, the alloying elements are not evenly distributed and particularly

the center is solute-depleted of Mg and Mn. This may be another reason for the very coarse grains observed at the center of the ingot.

The grain size evolution with cooling rate observed in this study is qualitatively in good agreement with previous works on DC casting by Erdegren et al. [21], Nadella et al. [12] and Suyitno [22]. Erdegren et al. [21] found, on a DC cast 6xxx series alloy, an increase in grain size with increasing distance from the surface. However, Nadella et al. [12] and Nagayumi [23] found that in Al-Mg alloys the maximum and minimum grain sizes occur in the area adjacent to the center and in the subsurface region, respectively, not exactly at the center and the surface as is seen in Fig. 1.

3.2 Segregation

An analysis of the non-uniformity in the chemical composition across the cross section of the samples was done using EDS analysis. As is known, the prominent constituent elements of AA5182 are Mg (3.92wt.%) and Mn (0.38 wt.%). Additionally, the experimental alloy contained a small amount of Cr (0.18 wt%). The variation in the amount of alloying elements from the center to the surface of the experimental DC cast alloy is shown in Table 2. At the first glance, it is obvious that there is significant macrosegregation. This is due to fluid flow during casting, and solute rejection by the solid phase (partitioning of solute elements between liquid and solid) during solidification. In order to quantify the macrosegregation of alloying elements in different locations, the deviation from the nominal (average) composition ($\frac{[X]-[X]_{nominal}}{[X]_{nominal}}$) is used as a representative of segregation, where [X] is the composition of element X and $[X]_{nominal}$ is the nominal composition of element X in the ingot. Fig. 2 shows the deviation from nominal composition of each alloying element at different distances from the center. Values greater than zero of this deviation imply 'positive' macrosegregation and conversely, values less than zero indicate 'negative' macrosegregation.

As can be seen in Fig. 2, Mg has considerable negative macrosegregation at the center of the ingot. This is in line with the results of previous studies on DC cast billets and ingots by Erdegren et al. [21] and Eskin et al. [24]. The observed centerline segregation is likely attributed to solutal convection. Based on this mechanism, small particles of lower solute concentration detach from the first solidified shell and settle at the center causing macrosegregation. The particles settle since they have a higher density due to a lower Mg content and fall towards the base of the sump due to gravity. One can also see a small positive segregation of Mg close to the chill surface. This phenomenon is most likely due to the presence of liquid richer in solute within the interdendritic channels close to the surface during

solidification as suggested by Erdegren et al. [21]. Due to solidification shrinkage, liquid of higher concentration away from the surface is sucked back into these channels, thus solidifying with a higher concentration of Mg and resulting in a positive segregation of Mg close to the chill surface.

Similar to Mg, Mn also shows negative segregation at the centerline, due to solutal convection, and positive segregation between the center and the surface. However, contrary to Mg, Mn shows negative segregation at the surface of the ingot. This phenomenon has not been seen before as Eskin et al. [24], and Nadella et al. [25] found positive segregation of Mn in DC cast ingots, while Dons et al. [26] observed that manganese resists macrosegregation in DC cast Al-Si alloys. Finally Cr shows a positive segregation at the center, no segregation at the middle and negative segregation at the surface of the ingot.

The segregation of Mg and Mn away from the center of the casting and for Cr towards the center is in line with the expected behavior based on their partition coefficients, k, in a binary alloy with Al. In general, it has been reported (e.g. [12]) that alloying elements with $k<1$ such as Mg and Mn show a solute-depleted centerline segregation, while elements with $k>1$ such as Cr exhibit the opposite pattern. The extent of the segregation can be associated to magnitude of the partition coefficient. Values close to 1, like for Mn (k~0.9) show only slight segregation, while small values, like for Mg (k~0.4), show strong centerline segregation.

3.3 Thermal analysis

Fig. 3 shows the DSC signals of the material during solidification under cooling rate of 10 °C/min. Because the solidification phenomenon is an exothermic reaction, the curve takes a downward path. As can be seen, the liquidus is easily identifiable on the right side of the curve at ~636 °C. To estimate the solidus point, a third order polynomial baseline was drawn with the points well above the liquidus and well below the expected solidus. The intersection point of this baseline with this curve provides a good estimate of the solidus, which is estimated to be ~510 °C. Besides these two points, one can see two obvious deviations in the middle part of the curve, which correspond to the eutectic reaction and the formation of precipitates. During cooling the material from fully liquid state, the primary α phase nucleates and begins to solidify at a temperature of about 636 °C. Upon further cooling to 591 °C, the liquid goes through a eutectic reaction, in which a eutectic of α(Al) and Al_6(FeMn) forms. Finally, at a temperature of ~561 °C the Mg_2Si phase is observed to precipitate.

The observed sequence of solidification for AA5182 is in line with the findings of Thompson et al. [27] during solidification of the same alloy. However, in addition to these

reactions, Arnberg et al. [28] and Backerud et al [29] also reported the formation of a complex eutectic of ($Al+Mg_2Si+Al_3Fe+Al_8Mg_5$). This reaction was not observed in the current study, nor in the work by Thompson [27]. Thompson argued that the peak identified in [28] and [29] as the main eutectic reaction was actually caused by a strong temperature recalescence and subsequent plateau due to nucleation and growth of the primary phase. This argument was supported in [27] through examination of micrographs, which showed that the primary α-Al dendrites occur about 80-90% of the microstructure. The DSC curve presented in Fig. 3 also provide further evidence that the solidification of AA5182 contains only two main reactions, in addition to the liquidus temperature, since the curve only contains two deviations. The main reactions observed in the present thermal analysis can thus be summarized as:

T_L: Start of solidification and formation of α-Al

R_1: Start of eutectic reaction as $L \rightarrow \alpha(\mathrm{Al}) + \mathrm{Al}_6(\mathrm{MnFe})$

R_2: Precipitation of Mg_2Si as $L \rightarrow \alpha(\mathrm{Al}) + \mathrm{Mg}_2\mathrm{Si}$

In a same manner as the method for grain size and segregation studies, samples were taken from different locations between the centerline and the chill-surface for thermal analysis. The solidification behavior of these samples was then analysed. Three tests were run at each location. The resulting DSC traces are shown in Fig 4. It is clear from the figures that the samples of the three positions (center, middle and surface) show different solidification behavior in such a way that there are some shifts in liquidus, eutectic and precipitation with variation in position. As the distance from the surface increases, all these points shift to lower temperatures, although there is virtually no difference in the solidification curves for the 'middle' and the 'center' samples. The liquidus, solidus and the solidification reactions R_1 and R_2 along with their range of variation within the same location are listed in Table 3. For comparison purpose, the reaction temperatures determined by Thompson, Arnberg, and Bakerud [27-29] are also included in the table, with the assumption that only two secondary reactions are occurring during solidification.

It can also be observed from Fig. 4 that there is more latent heat evolved at the surface position as compared to the middle and centre. One possible hypothesis relates to the amount of micro-segregation. The largest negative segregation for Cr and Mn, is seen to occur at the surface, Fig. 2, which would increase the total amount of Al and Mg in this region. Since Al and Mg have the highest latent heat (the latent heat of the main elements are: Al ≈390, Mg

≈360, Cr ≈330, Mn ≈260, all in kJ/kg), this could lead to higher total latent heats of solidification.

The results in Table 3 indicate that the liquidus and the R_1 point are invariant with position within the level of uncertainty estimated by the standard deviation, while the R_2 and the solidus are sensitive to casting location. Specifically, the R_2 temperature increases slightly from surface to center, and the solidus point decreases considerably, by 6 deg., from the surface to the center. In addition, the reaction points are reproducible, as the standard deviation is less than two degrees. The variation in solidus temperature is most likely due to the high negative macrosegregation of Mg and Mn at the center, and positive segregation of Mg at the surface. This change in solidus with respect to position could have an important influence on hot tear formation in DC casting, since metals with a longer solidification regime are known to be more susceptible to hot tearing. Thus, we hypothesize that not only are certain regions of an ingot or billet more susceptible to hot tearing because of their sump depth and hence liquid feeding difficulties but also because macrosegregation will have resulted in compositional variations that depress the solidus temperature and extend the temperature window vulnerable to hot tearing.

The evolution in solid fraction with temperature is also important during casting. This can be determined by calculating the area under the curve between solidus and liquidus and is shown in Fig 5 as a function of position along the centerline. There is a difference in the evolution in fraction solid at different distances from the center. The fraction solid evolution of the sample taken from center and the middle are almost identical, owning to similar DSC curves, while that of the sample at the surface is quite different. This was expected given the results in Table 3 as the change in location from center and middle to surface (and in turn change in the local composition) depressed the precipitate formation temperature and increased the solidus temperature. This limited the temperature interval and in turn the volume fraction of solid formed during the last stages of solidification for the surface sample.

In previous paragraphs, the capability of thermal analysis in studying the effect of macrosegregation on the solidification behavior of a DC cast AA5182 ingot was examined. In addition, thermal analysis can be used to physically simulate casting under different cooling rates. For this purpose two samples taken from the surface of the ingot were tested in the DSC, at 10˚C/min and 20˚C/min cooling rates. The liquidus, solidus, and reaction temperatures for these two cooling rates have been summarized in Table 4, while the corresponding curve showing the evolution in fraction solid is given in Fig. 6. It is seen that the liquidus points occur at the same temperature for both cooling rates within the level of uncertainty estimated by the

standard deviation, but the reaction and solidus temperatures are shifted towards lower temperatures for the higher cooling rate.

The experimental grain size, macrosegregation, and thermal analysis measurements performed in this study demonstrate the highly variable nature of such quantities in the DC casting process. This knowledge is important in the field of semisolid processing, since accurate prediction of defects requires localized knowledge of microstructural effects like alloy composition and impurities that will be strongly linked to the solidification behavior as well as the macroscale effects like segregation and cooling rate. The results of the current work indicate that the critical points such as the solidus as well as the eutectic and precipitate formation temperature vary as a function of cooling rate and local chemical composition. These would alter the mechanical behavior of the mush. Future process models of DC casting should thus take this variation in mechanical behaviour into account to improve semi-solid stress/strain predictions.

4. Conclusions

The evolution in grain size and macrosegregation as well as the solidification sequence of a direct chill cast AA5182 have been studied in the current work. The main findings are as follows.

- Grain size is found to increase substantially from the surface to the center of the ingot, due to the significant variation in cooling rate.
- There is strong macrosegregation of Mg, Mn and Cr from center to surface due to fluid flow and partitioning of solute elements between liquid and solid during solidification. Mg shows negative segregation at the center and positive segregation at the surface. Mn shows negative segregation both at center and surface, and positive segregation elsewhere. Cr shows positive segregation at the center and negative segregation at the surface.
- The sample location within a DC cast ingot influences the solidus and reactions temperatures, as well as the evolution in fraction solid, mostly due to localized difference in chemical composition.
- The nucleation temperatures of the different phases showed different trends with variation in cooling rate in such a way that the liquidus temperature remains constant, but the formation

temperatures of the eutectic and precipitate as well as the solidus temperature were depressed by increasing the cooling rate.

Acknowledgments

The authors would like to thank the financial support of the Natural Sciences and Engineering Research Council (NSERC) of Canada.

References

[1] D. Carle, B. Gordon, The Suitability of Aluminium as an Alternative Material for Car Bodies, *Mater. Des.* 1999, 20, p 267-272

[2] S. Das, W. Yin, Trends in the Global Aluminum Fabrication Industry, *JOM*, 2007, 59, p 83-87

[3] D. Stefanescu, The New Metals Hand Book: Volume 15, *Casting*. ASM International, 1988

[4] W.E. Droste, G.U. Grun, W. Schneider, J.M. Drezet, Thermo-mechanical Modeling to Predict Shrinkage, Shape and Mold Openings for DC-cast Rolling Ingots, *Light Metals TMS*, 2002, pp 703-708

[5] S. Benum, D. Mortensen, H. Fjaer, H. Overlie, O. Reiso, On the Mechanism of Surface Cracking in DC Cast 7xxx and 6xxx Extrusion Ingot Alloys. *Light Metals TMS*, 2002, pp 967-974

[6] J. Sengupta, S.L. Cockcroft, D.M. Maijer, M.A. Wells, A. Larouche, On the Development of a Three-dimensional Transient Thermal Model to Predict Ingot Cooling Behavior During

the Start-up Phase of the Direct Chill-casting Process for an AA5182 Aluminum Alloy Ingot. *Metal. Mater. Trans. B*, 2004, 35, p 523-540

[7] A.B. Phillion, S.L. Cockcroft, P.D. Lee, X-ray Micro-tomographic Observations of Hot Tear Damage in an Al–Mg Commercial Alloy. *Scripta Mater*., 2006, 55, p 489-492

[8] A.B. Phillion, S.L. Cockcroft, P.D. Lee, A New Methodology for Measurement of Semi-solid Constitutive Behavior and its Application to Examination of As-cast Porosity and Hot Tearing in Aluminum Alloys. *Mater. Sci. Eng. A*, 2008, 491, p 237-247

[9] J. Drezet, M. Rappaz, Modeling of Ingot Distortions During Direct Chill Casting of Aluminum Alloys, *Metal. Mater. Trans. A*, 1996, 27, p 3214-3225.

[10] A. Williams, T. Croft, M. Cross, Modeling of Ingot Development During the Start-up Phase of Direct Chill Casting, *Metal. Mater. Trans. B*, 2003, 34, p 727-734

[11] N. Jamaly, A.B. Phillion, J.M. Drezet, Stress–Strain Predictions of Semisolid Al-Mg-Mn Alloys During Direct Chill Casting: Effects of Microstructure and Process Variables, *Metal. Mater. Trans. B*, 2013, 44, p 1287-1295

[12] R. Nadella, D. Eskin, Q. Du, L. Katgerman, Macrosegregation in Direct-chill Casting of Aluminium Alloys. *Prog. Mater. Sci.*, 2008, 53, p 421-480.

[13] D.G. Eskin, R. Nadella, L. Katgerman, Effect of Different Grain Structures on Centerline Macrosegregation During Direct-chill Casting. *Acta Mater.*, 2008, 56, p 1358-1365

[14] D.G. Eskin, V.I. Savran, L. Katgerman, Effects of Melt Temperature and Casting Speed on the Structure and Defect Formation During Direct-chill Casting of an Al-Cu Alloy, *Metal. Mater. Trans. A*, 2005, 36, p 1965-1976

[15] A.M. Glenn, S.P. Russo, P.J.K. Paterson, The Effect of Grain Refining on Macrosegregation and Dendrite Arm Spacing of Direct Chill Cast AA5182. *Metal. Mater. Trans. A*, 2003, 34, p 1513-1523

[16] H.B. Dong, R. Brooks, Determination of Liquidus Temperature in Al–Si and Al–Si–Mg Alloys Using a Single-pan Scanning Calorimeter, Mater. Sci. Eng. A, 2005, 413, p 480-484

[17] ASTM E112-10, *Standard Test Methods for Determining Average Grain Size*, ASTM International, West Conshohocken, PA, 2010

[18] D. E. Newbury, N.W.M. Ritchie, Is Scanning Electron Microscopy/Energy Dispersive X-ray Spectrometry (SEM/EDS) Quantitative?, *Scanning*, 2013, 35(3), p 141-168

[19] M.A. Easton, D.H. StJohn, An Analysis of the Relationship Between Grain Size, Solute Content, and the Potency and Number Density of Nucleant Particles, *Metal. Mater. Trans. A*, 2005, 36, p 1911–1920

[20] D.G. Eskin, Q. Du, D. Ruvalcaba, L. Katgerman, Experimental Study of Structure Formation in Binary Al–Cu Alloys at Different Cooling Rates. *Mater. Sci. Eng. A*, 2005, 405, 1-10

[21] M. Erdegren, M.W. Ullah, T. Carlberg, Simulation of Surface Solidification in Direct-Chill 6xxx Aluminum Billets, *IOP Conference Series: Materials Science and Engineering*, 2011, 27, p 012013

[22] Suyitno, *Hot Tearing and Deformation in Direct Chill Casting of Aluminum Alloys*. Ph.D. thesis, 2005, Delft University of Technology.

[23] H. Nagaumi, Prediction of Porosity Contents and Examination of Porosity Formation in Al-4.4Mg DC Slab, *Science and Technology of Advanced Materials*, 2001, 2, p 49-57

[24] D.G. Eskin, Suyitno, L. Katgerman, Mechanical Properties in the Semi-Solid Sate and Hot Tearing of Aluminum Alloys, *Prog. Mater. Sci.*, 2004, 49, p 629-711

[25] R. Nadella, D.G. Eskin, L. Katgerman, Effect of Grain Refinement on Structure Evolution, Floating Grains, and Centerline Macrosegregation in Direct-Chill Cast AA2024 Alloy Billets, *Metal. Mater. Trans. A*, 2008, 39, p 450-461

[26] A. Dons, L. Pedersen,L. Arnberg, The Origin of 'Anomalous' Microsegregation in Al-Si Foundry Alloys - Modelling and Experimental Verification, *Mater. Sci. Eng. A*, 1999, 271, p 91-94

[27] S. Thompson, S.L. Cockcroft, M. Wells, Effect of Cooling Rate on Solidification Characteristics of Aluminium Alloy AA5182, *Mater. Sci. Technol.*, 2004, 20, p 497-504

[28] L. Arnberg, L. Backuerud, G. Chai, Solidification Characteristics of Aluminum Alloys, Volume 3 : Dendrite Coherency. Number v. 3 in Solidification Characteristics of Aluminum Alloys, AFS/Skan aluminium, 1996

[29] L. Backuerud, G. Chai, J. Tamminen, Solidification Characteristics of Aluminum Alloys,Volume 2:Foundry Alloys. 3rd edition, AFS Skanaluminium, Stockholm, Sweden, J. 1990

Figures and Tables

Figure 1: Optical micrographs of samples taken from (a) center, (b) 62.5 mm (c) 125 mm, and (d) at surface of the ingot, viewed under cross-polarized light with sensitive tint attachment.

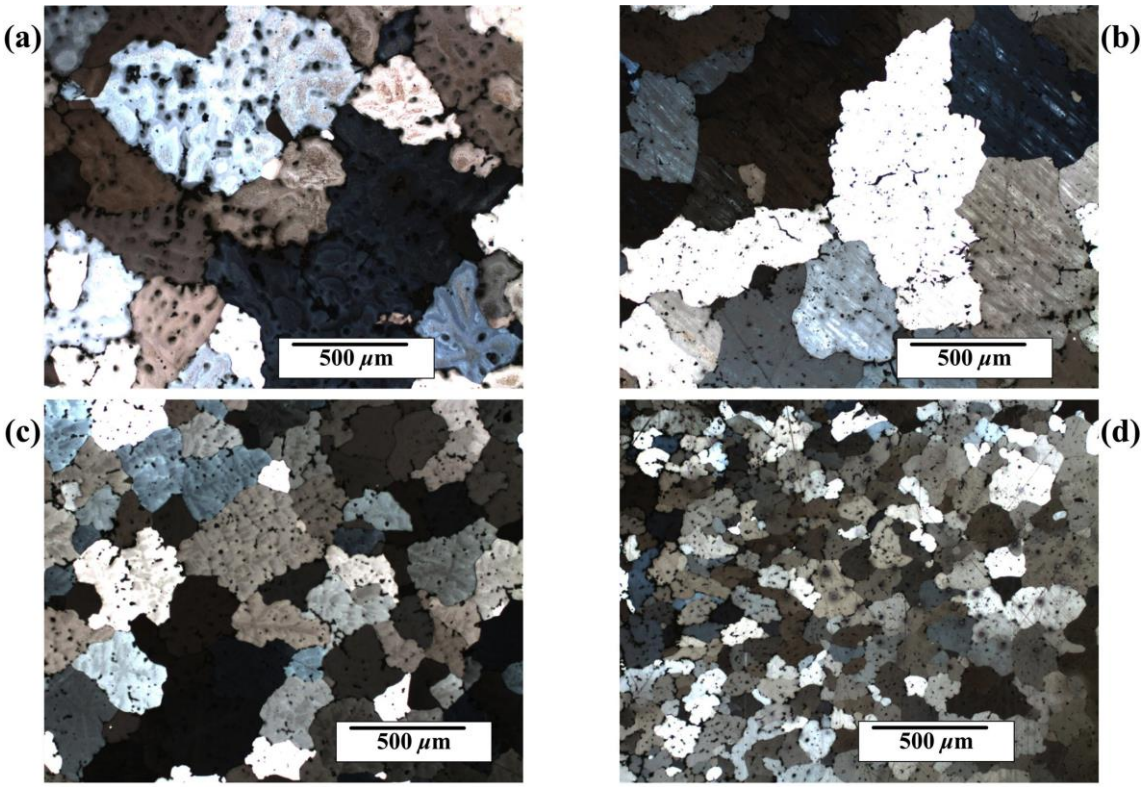

Figure 2: Distribution of relative concentration of different alloying elements a function of distance from the center of the ingot.

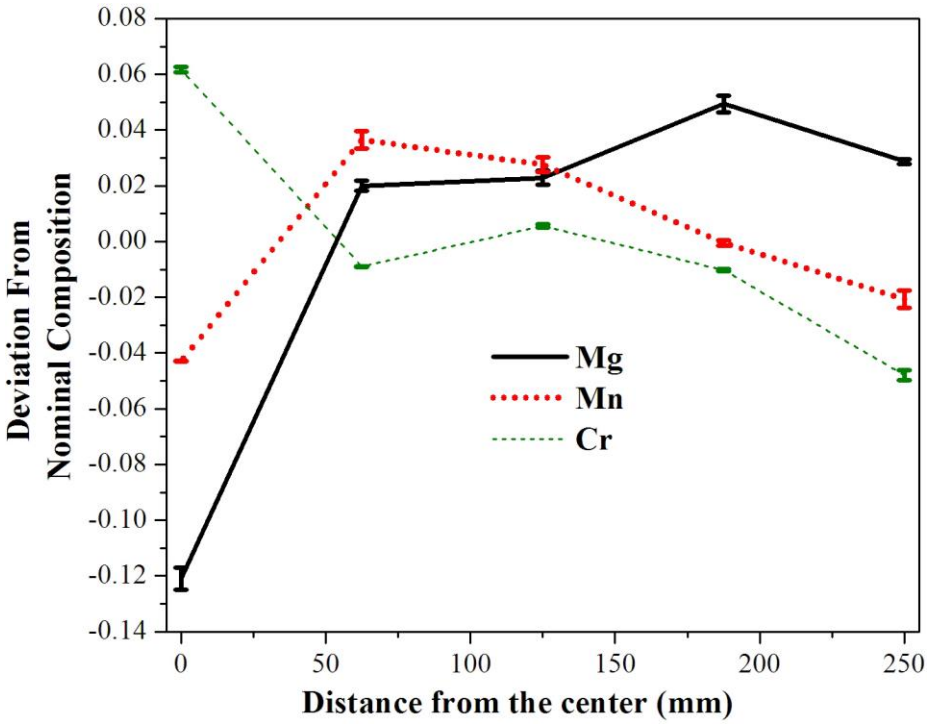

Figure 3: DSC curve of a sample of as-cast AA5182 from the DC cast ingot (middle position), cooling rate = 10˚C/min. The dashed line represents the third-order polynomial drawn in the single phase regions.

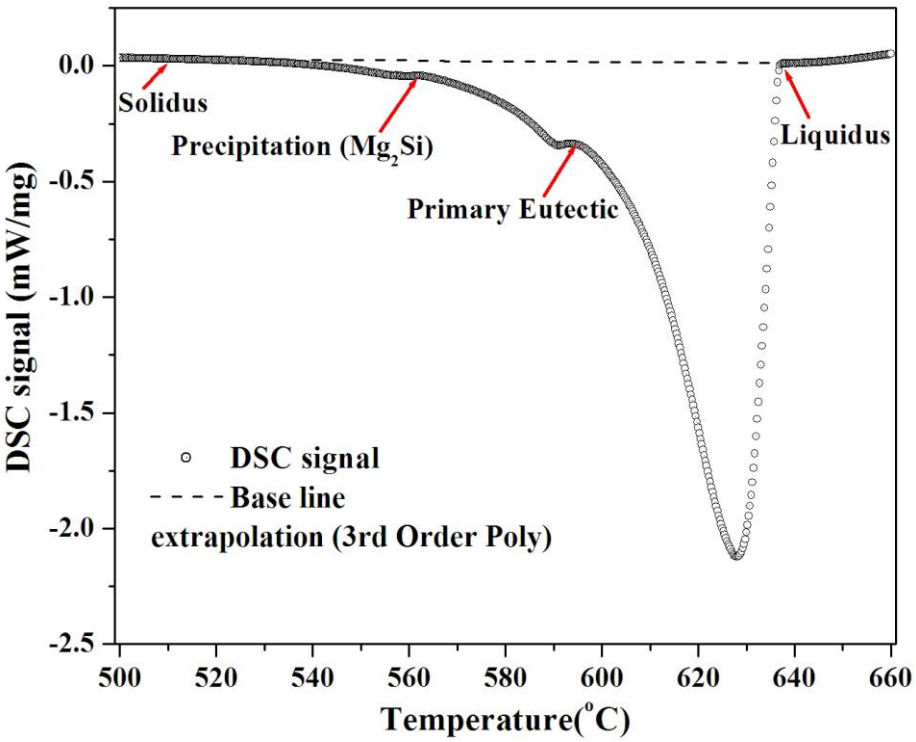

Figure 4: DSC curves of samples of as-cast AA5182 taken from different locations within the ingot, cooling rate = 10˚C/min.

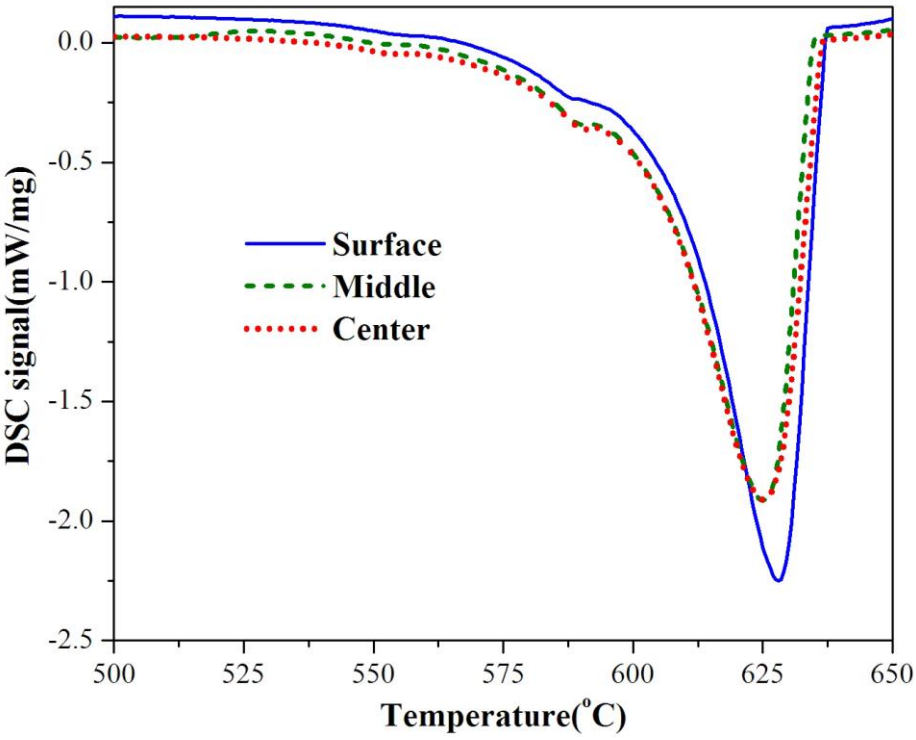

Figure 5: Solidification path of samples of as-cast AA5182 taken from different locations within the ingot, cooling rate = 10˚C/min.

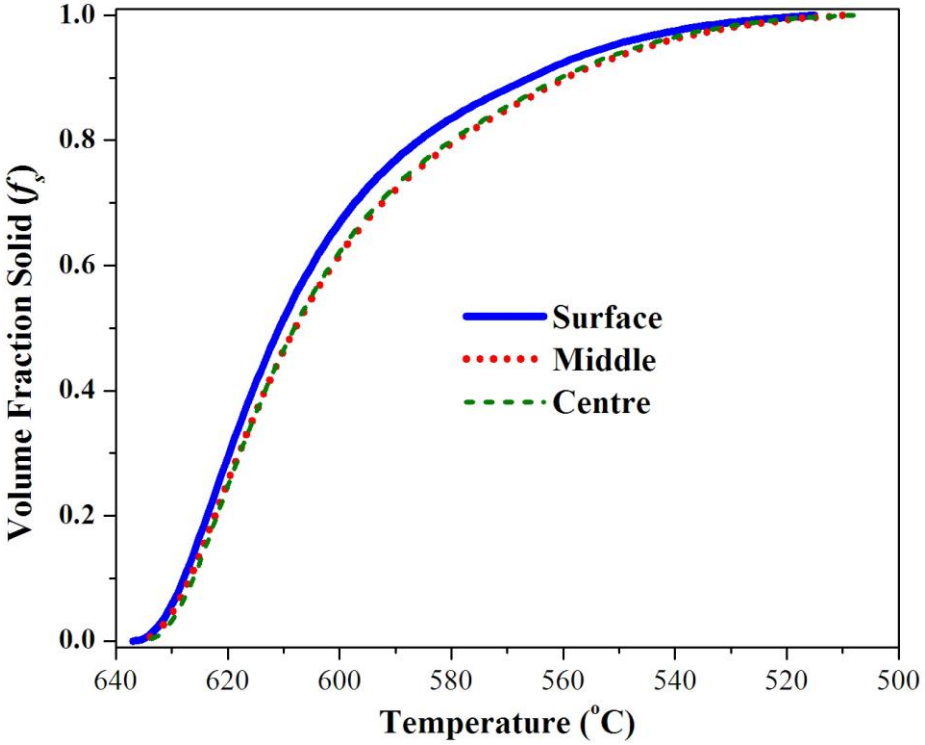

Figure 6: Solidification path of samples of as-cast AA5182 taken from the surface of the ingot, cooled as (a) 10˚C/min and (b) 20˚C/min.

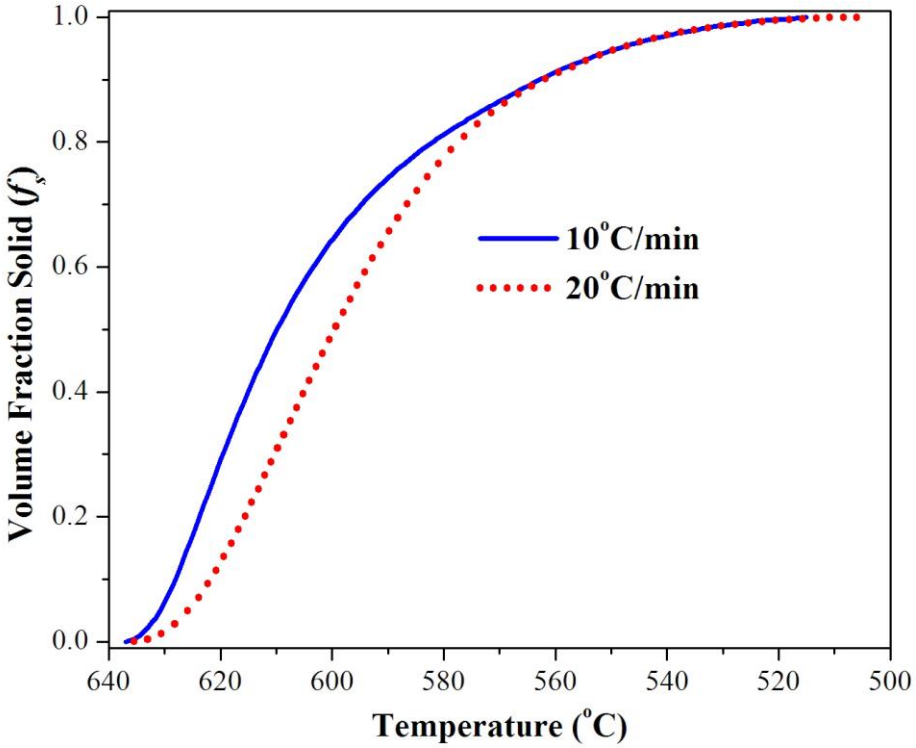

Table 1: Average grain size, $\bar{d}$, of as a function of distance from the centre of the ingot

Position Relative to Ingot Center (mm)	$\bar{d}$ (mm)	S.D.[1]
0	515	31
62	394	27
125	257	28
187	257	38
250 (surface)	123	20

[1]Standard Deviation

Table 2: Average compositions of major alloying elements as a function of distance from the centre of the ingot

Position Relative to Ingot Center (mm)	Alloying Element (wt%)		
	Mg	Mn	Cr
0	3.45	0.37	0.19
62	4.00	0.40	0.18
125	4.01	0.39	0.18
187	4.11	0.38	0.18
250 (surface)	4.03	0.38	0.17

Table 3: Comparison of averaged solidus, liquidus, and solidification reaction temperatures of as-cast AA5182 to [27][28][29]. Note that the experimental values from this work correspond to a cooling rate of 10˚C/min. Note also that the standard deviation for each data point is shown in parenthesis. All temperatures in ˚C

Source	T_L	R_1	R_2	T_S
Exp. (center; 0 mm)	635 (2)	592 (2)	564 (1)	508 (1)
Exp. (middle; 125 mm)	636 (2)	591 (2)	561 (1)	510 (2)
Exp. (surface; 250 mm)	636 (1)	591 (1)	557 (2)	514 (2)
Ref. 28	637	582	560	536
Ref. 29	632	586	557	470
Ref. 27	624	587	557	508

Ref.28: Arnberg et al., Cooling rate=18 ˚C/min
Ref.29: Bakerud et al., Cooling rate=18˚C/min
Ref.27: Thompson et al., Cooling rate=30 ˚C/min

Table 4: Comparison of solidus, liquidus, and solidification reaction temperatures of as-cast AA5182 as a function of cooling rate. Note that the standard deviation for each data point is shown in parenthesis. All temperatures in ˚C

Source	***CR* (˚C/min)**	T_L	R_1	R_2	T_S
Exp. (surface position)	10	636 (1)	591 (1)	557 (2)	514 (2)
Exp. (surface position)	20	637 (1)	590 (2)	556 (1)	504 (1)
Ref. 29	18	632	586	557	470
Ref. 29	54	632	584	556	470

Ref.29: Bakerud et al., Cooling rates=18 and 54 K/min